Breakdown of Shape Memory Effect in Bent Cu–Al–Ni Nanopillars: When Twin Boundaries Become Stacking Faults

Article *in* Nano Letters · December 2015

DOI: 10.1021/acs.nanolett.5b03483

CITATIONS
2

READS
147

5 authors, including:

Xiangdong Ding
Xi'an Jiaotong University
153 PUBLICATIONS **1,664** CITATIONS
SEE PROFILE

Liu Juan
Henan University of Science and Technology
208 PUBLICATIONS **3,821** CITATIONS
SEE PROFILE

Ekhard Salje
University of Cambridge
621 PUBLICATIONS **14,580** CITATIONS
SEE PROFILE

NANO LETTERS

Letter

pubs.acs.org/NanoLett

Breakdown of Shape Memory Effect in Bent Cu−Al−Ni Nanopillars: When Twin Boundaries Become Stacking Faults

Lifeng Liu,[†,‡] Xiangdong Ding,[*,†] Jun Sun,[†] Suzhi Li,[†] and Ekhard K. H. Salje[*,†,§]

[†]State Key Laboratory for Mechanical Behavior of Materials, Xi'an Jiaotong University, Xi'an 710049, China

[‡]State Key Laboratory of Nonlinear Mechanics, Institute of Mechanics, Chinese Academy of Sciences, Beijing 100190, China

[§]Department of Earth Sciences, University of Cambridge, Cambridge CB2 3EQ, United Kingdom

ABSTRACT: Bent Cu−Al−Ni nanopillars (diameters 90−750 nm) show a shape memory effect, SME, for diameters $D > 300$ nm. The SME and the associated twinning are located in a small deformed section of the nanopillar. Thick nanopillars ($D > 300$ nm) transform to austenite under heating, including the deformed region. Thin nanopillars ($D < 130$ nm) do not twin but generate highly disordered sequences of stacking faults in the deformed region. No SME occurs and heating converts only the undeformed regions into austenite. The defect-rich, deformed region remains in the martensite phase even after prolonged heating in the stability field of austenite. A complex mixture of twins and stacking faults was found for diameters 130 nm $< D <$ 300 nm. The size effect of the SME in Cu−Al−Ni nanopillars consists of an approximately linear reduction of the SME between 300 and 130 nm when the SME completely vanishes for smaller diameters.

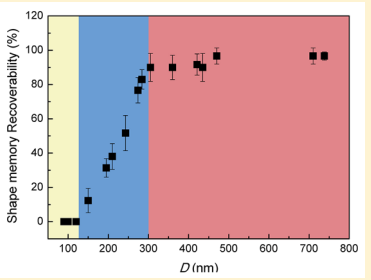

KEYWORDS: *finite size scaling, shape memory effect, size dependence of shape memory, twinning, stacking faults, Cu−Al−Ni alloys*

All ferroic materials show finite size effects when sample dimensions decrease below some characteristic lengths and the ferroic effect is destroyed. Such length scales exist in magnetism,[1−4] whereas finite size effects in ferroelectrics are primarily related to the depolarization field,[5−8] which tends to destroy the formation of the spontaneous polarization. The typical geometries in ferroelectrics are thin films (critical thickness is 10 nm[9,10]) and thin polymer layers (critical thickness is 2.5 nm[11−14]). Finite size effects are also expected in ferroelastic (martensitic) materials and nanoscale shape memory alloys (SMAs).[15−20] Here, the ideal geometry for investigations is nanopillars[21−24] to identify the minimum diameter below which the shape memory effect (SME) is destroyed. Structural arguments lead to such an expectation because the induced nanostructures will change with size: bending of nanopillars will always lead to the formation of suitable adaptive nanostructures,[25] but only some nanostructures, namely twins, contribute to the SME, whereas others do not. If strain-induced twinning disappears below a certain length scale, no SME can exist at smaller lengths. Furthermore, complex nanostructures may impede the phase transformation to the austenite phase under heating and thereby also destroy the SME.

We report experimental observations that show that finite size effects in sheared nanocolumns stem indeed from a crossover between twinning in thicker nanopillars to sequences of disordered stacking faults in thinner ones. This result has considerable technological relevance for the applications of superelastic and shape memory effects[19,20] and the use of SMAs in nanoscale device applications.[26,27] Furthermore, it shows a size-limit for the generation of twin-wall-related functionalities such as polar twin walls,[25] because the template for polarity, namely the twin wall itself, becomes unstable below a critical thickness of the nanopillar. This prevents us from the development of high-density ferroelectric memory devices based on twinned nanopillars with polar twin boundaries.[28] Previous investigations on submicron SMAs[29−31] with diameters 200−300 nm failed to identify the breakdown of the SME. Here, we show that the critical diameter for the breakdown of the SME is indeed smaller than 200 nm.

Investigations of size dependent mechanical twinning under compression have already revealed some grain-size dependence.[32−42] The grain size effect of twinning has been reported in nanocrystalline Ni and Cu[33,38] and has been attributed to the competition between the grain size-dependence of partial dislocations and the layer-by-layer promotion of partial slip near the surface. Hexagonal close-packed Ti−5%Al (atom %) crystal pillars show that the stress required for deformation twinning increases drastically for compression and samples sizes (~1 μm), below which twins are suppressed and replaced by dislocations.[36] Mechanical twinning in these experiments was driven by compression and studied in structural (non-SMA) materials. Our approach is different: first, we use bending deformations because most SME applications make use of bending rather than compression.[43−45] Second, mechanical twinning in conventional materials is different from transformation twinning in SMAs where the twin angles and twin wall energies tend to be much lower than in mechanical twinning. Hence, we cannot necessarily extrapolate the results from structural materials to SMAs and the size dependence of

Received: August 29, 2015
Revised: November 18, 2015

DOI: 10.1021/acs.nanolett.5b03483
Nano Lett. XXXX, XXX, XXX−XXX

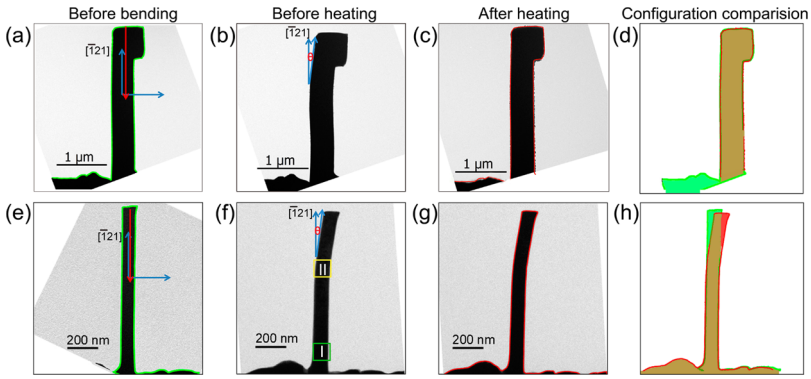

Figure 1. Shape memory behavior of nanopillars of Cu−13.8Al−4.2Ni with a bending axis $[\bar{2}11]$, the bending angle is $\theta_1 = 8.0°$ for large and $\theta_2 = 7.5°$ for thin pillars. (a)−(d) Shape recovery of a large pillar with sample thickness $D = 470$ nm, height 3326 nm (including the cane shape part). (e)−(h) Shapes of a thin pillar with $D = 90$ nm, height 1005 nm with no shape recovery after heating. The aspect ratio of the cross section of all pillars varies between 0.95 and 1.

the SME is expected to be rather different from that of mechanical twinning experiments.

We used a JEM 2100F FEG transmission electron microscopy (TEM) with Hysitron PicoIndenter 95 (PI 95) system of Hystitron to measure the shape recovery of bent nano-SMA Cu−13.8Al−4.2Ni. We first fabricated pillars of different sizes using dual-beam focused-ion-beam (FIB) with a 30 kV gallium ion-beam and a 15 kV electron-beam. The current was controlled to be 1.5 pA to minimize the contamination of the sample by gallium. We achieved in-plane bending by off-axis compression of "cane shaped" samples (Figure 1). The length-to-thickness aspect ratios were about 8 for thicknesses D of the pillars (below the cane handle) between 270 and 750 nm. This same aspect ratio was ca. 11 for thinner samples with D between 90 nm and 250 nm. The aspect ratios of cross sections of all pillars varied between 0.95 and 1. The heating process was conducted inside a Gatan 628 Heating Holder. By controlling the electric current, the bent sample was heated to a given temperature and kept at that temperature for 20 min. We then checked any change of the sample shape and diffraction pattern and repeated the procedure every 30K. Final TEM observations at 573 K lasted for ca. 1.5 h. For the thinner pillar, which does not show SME, we heated the sample to 843 K and kept this temperature for 1 h. We then performed another TEM observation for a further

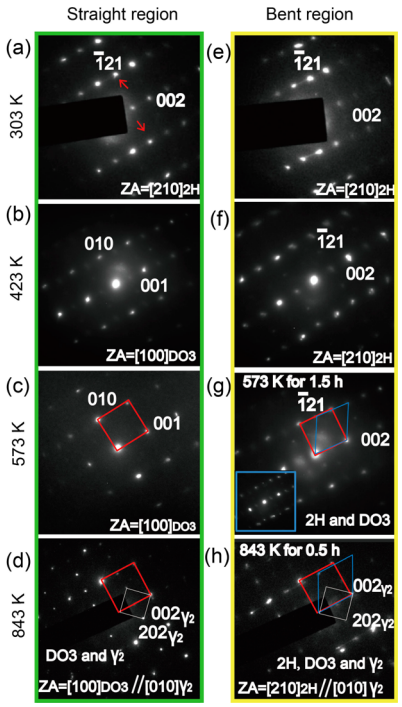

Figure 2. Diffraction patterns of straight (a, b, c, d) and bent (e, f, g, h) regions of a thin pillar during heating ($D = 90$ nm). SADP of the martensite 2H structure in the straight region at 303 K (a) and at 423 K (b). Complete transformation from martensite to austenite is seen by the disappearance of 2H reflections and the appearance of DO_3 reflections(b), complete recovery to DO_3 phase (red square)at 573 K (c), while γ_2 phase (white square) precipitates at 843 K (d). SADP of the bent region at 303 K (e) also shows that the 2H structure does not change after heating to 423 K (f). Some incomplete transformation is seen after heating to 573 K for 1.5 h (g). The inset in (g) shows the diffraction pattern directly after heating to 573 K with no recovery. After heating to 843 K for 1.5 hours (h), γ_2 precipitates, leading to the coexistence of 2H (blue parallelogram), DO_3 (red square), and γ_2 (white square) phases.

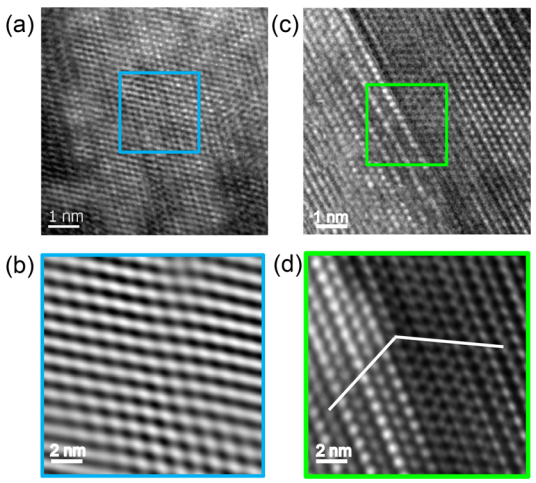

Figure 3. HRTEM of underformed pillars (a, b) and the bent region of a thick pillar (c, d). (a) Structure of underformed pillars and inverse fast Fourier transformation (IFFT) of the area in the blue frame (b) showing the ABABAB... stacking of the martensite 2H phase. Twins appear in the bent region of a thick pillar (c) and the IFFT (d) Twinned lattice planes are shown by white lines.

DOI: 10.1021/acs.nanolett.5b03483
Nano Lett. XXXX, XXX, XXX−XXX

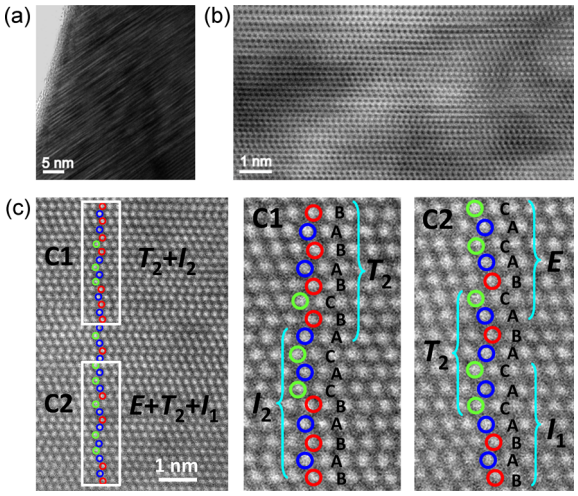

Figure 4. Atomic-resolution (S)TEM images of the bent region of a thin pillar (D = 90 nm). (a) Bright field TEM image of a region near the surface of the bent area showing a high density of stacking faults. (b) Bright field STEM image of (a) showing serious distortion of lattice due to the high density of stacking faults. (c) Dark field STEM image recorded at the interior of the bent area showing less distortion of lattice (compared to the severe distorted region (b)) and various stacking sequences (c), for example, $T_2 + I_2$, and $E + T_2 + I_1$ as shown in the insets C1 and C2.

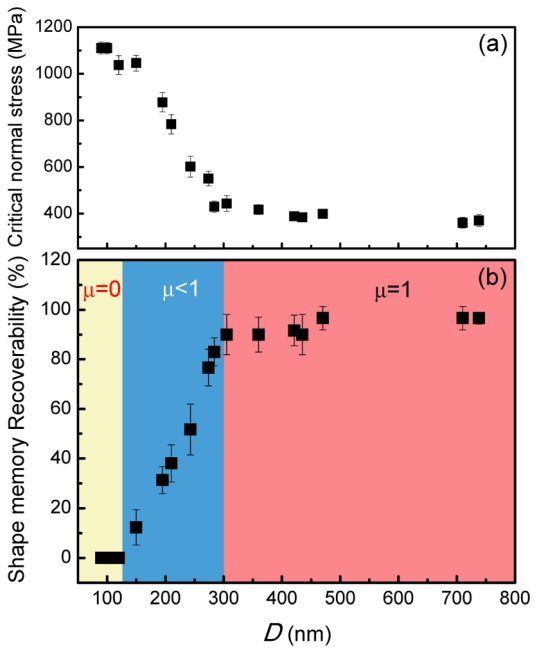

Figure 5. (a) Change of critical normal stress with sample thickness D. The critical normal stress is calculated by My/I, where M is maximum bending moment before yielding, y vertical distance away from the neutral axis, and I the moment of inertia of the cross-sectional area. (b) Finite size scaling of the degree of shape recovery in bent Cu–Al–Ni nanopillars. No shape recovery occurs below 130 nm, whereas full recovery occurs for sizes larger than 300 nm. In the intermediate crossover regime, we find a linear increase of the shape recovery with increasing size (recoverability $\mu = (\theta - \theta')/\theta'$, where θ and θ' are the bending angles before and after heating (see Figure 1).

0.5 h. In particular, in order to investigate the atomic stacking sequences of the stacking faults in the bent area, we prepared a thin specimen from one of the bent thin pillars (D = 90 nm) without heating, by using a Fischione 1040 NanoMill system. The atomic structure of the stacking faults was investigated on a JEM ARM200F spherical-aberration corrected microscope at 200 keV.

The off-axis compression leads indeed to the bending of the nanopillar as shown in Figure 1. The red and blue arrows were the load axis and the central axis along $[\bar{2}11]$, respectively. The bending angle θ is shown in Figure 1b and f. The load direction was along the long axis of the martensitic pillars, the loading rate was 10^{-3} s^{-1}. The sample was a single crystal Cu–13.8Al–4.2Ni (wt %). The transformation temperatures from the austenite phase (DO_3) to martensite are M_s = 318.02 K, M_f = 297.98 K, A_s = 303.19 K, and A_f = 328.86 K,[20] twin planes are $\{121\}_{2H}$.

Figure 1 shows that bent thick and thin nanopillars behave fundamentally differently. Full shape recovery under heating occurs for the thick samples (e.g., Figure 1a–d), whereas samples with thicknesses below 130 nm (Figure 1e–h) show no shape recovery and hence no SME. Selected area diffraction patterns (SADPs) were undertaken to explore the difference between the straight and bent areas of the thin nanopillar (Figures 1 and 2). The SADP of the straight parts of the nanopillars at room temperature always shows the martensitic 2H structure (Figure 2a of a 90 nm nanopillar). The transformation from the martensite phase to austenite is almost complete when the sample is heated to 423 K (Figure 2b, disappearance of the 2H reflections with [210] zone axis and the appearance of DO_3 reflections with [100] zone axis). A complete transformation to austenite DO_3 is seen after heating to 573 K (Figure 2c). The same transformation behavior was found for all thick nanopillars for both the straight and the bent regions.

This behavior is very different for the bent regions of thin nanopillars (diameter 90 nm in Figure 2e). The SADP at room temperature shows the martensitic 2H structure. The SADP still shows the 2H structure after heating to 423 K (Figure 2f). Subsequent heating to 573 K for 1.5 h only produced minor transformations into the austenite phase but no shape recovery (Figure 2g). The inset in Figure 2g shows the diffraction pattern with a high degree of martensitic deformation just after heating to 573 K. This observation proves that the bent region in this sample contains a large number of nonrecoverable defects, which prevent the transformation from martensite to austenite.

We further heated a thin nanopillar (D = 90 nm) to 843 K and kept it at that temperature for 1.5 h. We still do not find any shape recovery of the pillar. Instead, we find that a new phase γ_2 precipitated in both the straight and bent regions (Figure 2d and h). It is known that the appearance of the γ_2 phase hinders, or at least degrades, the shape memory effect of the CuAlNi alloys.[15] Thus, we cannot expect the SME to occur after the γ_2 precipitation.

The difference between the straight and bent regions in the thin nanopillars demonstrates that we are indeed investigating the size effect of the SME but not the size effect of the phase transformation between martensite and austenite. This latter size effect would be well below the thickness of our thinnest nanopillars (90 nm) because we find that the straight regions of all samples do indeed transform to austenite under heating. Only when the complex nanostructures are generated in the bent regions does the phase transformation to austenite and, hence, the SME disappear.

DOI: 10.1021/acs.nanolett.5b03483
Nano Lett. XXXX, XXX, XXX–XXX

The deformation mechanism for the thin and thick nanopillars is now analyzed by high-resolution transmission electron microscopy (HRTEM). Figure 3a and b show that the structure without lattice deformation is 2*H* in both the thin and thick nanopillars. However, in the bent region, only twinning occurs in the thick nanopillars (Figure 3c, d).

The bent region in the thin nanopillar (zone II in Figure 1f) contains complex polytypical stackings. The TEM image in Figure 4a and scanning TEM (STEM) image in Figure 4b show a high density of stacking faults near the surface of the bent area, whereas the density of the stacking faults is much lower at the interior of the bent area (Figure 4c). This implies that the stacking faults nucleate from the surface, and then propagate to the interior of the sample. This result is consistent with previous TEM observations of bent nanopillars in conventional structural materials,[36] where the nucleation of twins or dislocations under bending starts from the surface where the bending normal stress is largest. Detailed analysis of the STEM images shows that the stacking faults in the bent area involve four types, the intrinsic faults I_1 and I_2 with the stacking sequences ...ABABCBCBC... and ...ABABCACAC..., the extrinsic fault E with the stacking sequence ...ABABCABAB..., and the twin-like fault T_2 with the stacking sequences ...ABAB CBABA.... The combination of these stacking faults leads to polytypic stacking sequences with different repetition units (Figure 4b and c). These observations indicate that twinning deformation in thicker samples is replaced by highly disordered stackings in thin nanopillars. Disordered stackings are non-recoverable defects, which suppress the martensite to austenite transformation and hence the SME (in contrast to twins in thicker nanopillars).[46]

The breakdown of the SME, hence, has nothing to do with the length scale of elastic correlations or with the length scale of twin boundary interactions with the surface. Instead, we find that bending generates twin boundaries for large samples and complex stacking sequences for thin samples. The energy of twin boundaries is typically slightly smaller than that of stacking faults so that it is not surprising that bulk effects will favor twins (including their surface relaxation[47]), whereas thin samples favor stacking faults and polytypic transformations. This result can be rationalized by our understanding that twinning minimizes the global strain energy and, hence, is largely independent of the atomic configurations. Changes of stacking sequences minimize the local atomic interaction potentials but not the global strain energy. With decreasing size, surface relaxations reduce the strain energy so that now the local atomic energies become predominant and favor the development of local stackings. It is also well stablished that both twins and stacking faults are common in Cu−Al−Ni.[48] A previous microscopic model explains the inhibition of the martensitic transformation in bulk Cu−Al−Ni, related to the localized interaction between a dislocation array and the twinned 2*H* structure. This model takes into account the interaction between the martensitic stress-free transformation strains and the stress field created by the dislocation arrays.[49,50] Interactions between twin boundaries and stacking faults[51] and changes of stacking sequences during the martensitic transformation in Cu−Zn−Al SMAs are reported in ref 52 and the coexistence of twins and stacking faults in ref 53.

The transition, with decreasing sample size, from twinning to stacking faults may also be reflected by another approach based on the nucleation process of twins and stacking faults. It has been argued that twinning progresses via partial dislocations and the plane-to-plane propagation of partial dislocation slips.[35−39] It was then shown that these two steps have opposite size dependence,[36−39] namely small sample sizes increase the probability of first partial dislocations while decreasing the probability of plane-to-plane propagation of partial dislocation slips. On average, it seems that smaller sample sizes will suppress twinning in this model.

We also calculated the critical normal stress of the bent pillars with different size. The results in Figure 5a show that the critical normal stress under bending increases with the reduction of sample size. This is similar to the size dependence of the critical shear stress for twinning in ferroelastic materials.[54]

In summary, the finite size scaling of the SME is a consequence of the mixture of these two features: twinning is reversible under heating to the austenite phase but disordered stacking faults are not and even prevent the phase transformation altogether. In the intermediate regime, stacking faults may prevent twins from moving[55] and partially stabilize the 2H structure. The experimentally determined size dependence of the SME is shown in Figure 5b. No size dependence was found for samples with diameters larger than 300 nm when the SME is generated by twinning. An approximately linear decay was found between 350 and 130 nm when the SME is reduced from 90% to zero. No SME was found for samples thinner than 130 nm with complex stacking sequences dominating the bent regions. Applications of SMAs in miniaturized micro- and nanoelectromechanical systems (MEMS/NEMS), hence, are limited to samples bigger than the cutoff length (here 130 nm). Twin-wall-related functionalities also are impossible to observe in the thinnest nanopillars simply because twin walls cease to exist in the thinnest samples.

AUTHOR INFORMATION

Corresponding Authors

*E-mail: dingxd@mail.xjtu.edu.cn.
*E-mail: ekhard@esc.cam.ac.uk.

Author Contributions

X.D., J.S., and E.K.H.S. designed and supervised the project, L.F.L. carried out the in situ experiments and HRTEM experiments, S.L. analyzed the atomic-resolution STEM images. X.D. and E.K.H.S. wrote the paper. All authors contributed to discussion of the results.

Notes

The authors declare no competing financial interest.

ACKNOWLEDGMENTS

This work was supported by the National Natural Science Foundation of China (grant nos. 51171140, 51231008, 51321003, and 51320105014), the National Basic Research Program of China (grant no. 2012CB619402), the Program of Introducing Talents of Discipline to Universities in China (grant no. B06025), and The Engineering and Physical Sciences Research Council (grant no. EP/K009702/1). The authors thank "Jia-Lab for Interfaces and Atomic Structure" for letting us use spherical aberration-corrected (S)TEM, and intensive discussions. The authors also thank Xiaolei Wu for helpful discussion, Penghan Lu, Jian Zhang, and Shengwu Guo for the help on the in situ experiments.

DOI: 10.1021/acs.nanolett.5b03483
Nano Lett. XXXX, XXX, XXX−XXX

REFERENCES

(1) Kubota, T.; Mizukami, S.; Watanabe, D.; Wu, F.; Zhang, X.; Naganuma, H.; Oogane, M.; Ando, Y.; Miyazaki, T. *J. Phys. D: Appl. Phys.* **2013**, *46*, 155001.
(2) Ślęzak, M.; Ślęzak, T.; Freindl, K.; Karaś, W.; Spiridis, N.; Zając, M.; Chumakov, A. I.; Stankov, S.; Rüffer, R.; Korecki, J. *Phys. Rev. B: Condens. Matter Mater. Phys.* **2013**, *87*, 134411.
(3) Papaioannou, E. Th.; Kapaklis, V.; Taroni, A.; Marcellini, M.; Hjörvarsson, B. *J. Phys.: Condens. Matter* **2010**, *22*, 236004.
(4) Barrow, R. F. *Contemporary Physics*; Taylor & Francis LTD: Florence, KY, 1984; *25*, pp200−201.
(5) Scott, J. F.; de Araujo, C. A. P. *Science* **1989**, *246*, 1400−1405.
(6) Scott, J. F.; Duiker, H. M.; Beale, P. D.; Pouligny, B.; Dimmler, K.; Parris, M.; Butler, D.; Eaton, S. *Physica B+C* **1988**, *150*, 160−167.
(7) Zhong, W. L.; Wang, Y. G.; Zhang, P. L.; Qu, B. D. *Phys. Rev. B: Condens. Matter Mater. Phys.* **1994**, *50*, 698−703.
(8) Zhao, Z.; Buscaglia, V.; Viviani, M.; Buscaglia, M. T.; Mitoseriu, L.; Testino, A.; Nygren, M.; Johnsson, M.; Nanni, P. *Phys. Rev. B: Condens. Matter Mater. Phys.* **2004**, *70*, 024107.
(9) Karasawa, J.; Sugiura, M.; Wada, M.; Hafid, M.; Fukami, T.; Integr. *Ferroelectr* **1996**, *12*, 105−114.
(10) Ducharme, S.; Fridkin, V. M.; Bune, A. V.; Palto, S. P.; Blinov, L. M.; Petukhova, N. N.; Yudin, S. G. *Phys. Rev. Lett.* **2000**, *84*, 175−178.
(11) Choi, J. W.; Dowben, P. A.; Pebley, S.; Bune, A. V.; Ducharme, S.; Fridkin, V. M.; Palto, S. P.; Petukhova, N. *Phys. Rev. Lett.* **1998**, *80*, 1328−1331.
(12) Vizdrik, G.; Ducharme, S.; Fridkin, V. M.; Yudin, S. G. *Phys. Rev. B: Condens. Matter Mater. Phys.* **2003**, *68*, 094113.
(13) Ducharme, S.; Reece, T. J.; Othon, C. M.; Rannow, R. K. *IEEE Trans. Device Mater. Reliab.* **2005**, *5*, 720−735.
(14) Reece, T. J.; Ducharme, S.; Sorokin, A. V.; Poulsen, M. *Appl. Phys. Lett.* **2003**, *82*, 142−144.
(15) *Shape Memory Materials*; Otsuka, K., Wayman, C. M., Eds.; Cambridge University Press: New York, 1999; pp 27−101.
(16) Huang, W.; Ding, Z.; Wang, C.; Wei, J.; Zhao, Y.; Purnawali, H. *Mater. Today* **2010**, *13*, 54.
(17) Otsuka, K.; Ren, X. *Prog. Mater. Sci.* **2005**, *50*, 511−678.
(18) Ng, K.; Sun, Q. *Mech. Mater.* **2006**, *38*, 41−56.
(19) Liu, Y.; Li, Y.; Xie, Z.; Ramesh, K. *Philos. Mag. Lett.* **2002**, *82*, 511−517.
(20) Salje, E. K. H. *Annu. Rev. Mater. Res.* **2012**, *42*, 265−283.
(21) Maass, R.; Wraith, M.; Uhl, J. T.; Greer, J. R.; Dahmen, K. A. *Phys. Rev. E* **2015**, *91*, 042403.
(22) Gu, X. W.; Loynachan, C. N.; Wu, Z.; Zhang, Y.; Srolovitz, D. J.; Greer, J. R. *Nano Lett.* **2012**, *12*, 6385−6392.
(23) Gu, X. W.; Jafary-Zadeh, M.; Chen, D. Z.; Wu, Z.; Zhang, Y. W.; Srolovitz, D. J.; Greer, J. R. *Nano Lett.* **2014**, *14*, 5858−5864.
(24) Jang, D.; Li, X.; Gao, H.; Greer, J. R. *Nat. Nanotechnol.* **2012**, *7*, 594−601.
(25) Viehland, D. D.; Salje, E. K. H. *Adv. Phys.* **2014**, *63*, 267−326.
(26) Carpena-Nunez, J.; Yang, D.; Kim, J.; Park, C.; Fonseca, L. *Nanotechnology* **2013**, *24*, 035701.
(27) Lu, Y.; Peng, C.; Ganesan, Y.; Huang, J. Y.; Lou, J. *Nanotechnology* **2011**, *22*, 355702.
(28) Salje, E. K. H. *ChemPhysChem* **2010**, *11*, 940−950.
(29) San Juan, J.; No, M. L.; Schuh, C. A. *Adv. Mater.* **2008**, *20*, 272−278.
(30) Zhong, Y.; Gall, K.; Zhu, T. *Acta Mater.* **2012**, *60*, 6301.
(31) Clark, B. G.; Gianola, D. S.; Kraft, O.; Frick, C. P. *Adv. Eng. Mater.* **2010**, *12*, 808−815.
(32) Wu, X.; Zhu, Y. *Phys. Rev. Lett.* **2008**, *101*, 025503.
(33) Seo, J. H.; Park, H. S.; Yoo, Y.; Seong, T. Y.; Li, J.; Ahn, J. P.; Kim, B.; Choi, I. S. *Nano Lett.* **2013**, *13*, 5112−5116.
(34) Zhu, Y.; Liao, X.; Wu, X. *Prog. Mater. Sci.* **2012**, *57*, 1−62.
(35) Yu, Q.; Shan, Z. W.; Li, J.; Huang, X.; Xiao, L.; Sun, J.; Ma, E. *Nature* **2010**, *463*, 335−338.
(36) Yu, Q.; Qi, L.; Chen, K.; Mishra, R. K.; Li, J.; Minor, A. M. *Nano Lett.* **2012**, *12*, 887−892.
(37) Zhang, J. Y.; Liu, G.; Wang, R. H.; Li, J.; Sun, J.; Ma, E. *Phys. Rev. B: Condens. Matter Mater. Phys.* **2010**, *81*, 172104.
(38) Zhang, J. Y.; Wei, Y.; Sun, T.; Hartmaier, A.; Yan, Y.; Li, X. *Phys. Rev. B: Condens. Matter Mater. Phys.* **2012**, *85*, 054109.
(39) Zhang, J. Y.; Zhang, P.; Wang, R. H.; Liu, G.; Zhang, G. J.; Sun, J. *Phys. Rev. B: Condens. Matter Mater. Phys.* **2012**, *86*, 064110.
(40) Sedlmayr, A.; Bitzek, E.; Gianola, D. S.; Richter, G.; Monig, R.; Kraft, O. *Acta Mater.* **2012**, *60*, 3985−3993.
(41) Christian, J. W.; Mahajan, S. *Prog. Mater. Sci.* **1995**, *39*, 1−157.
(42) Minor, A. M.; Asif, S. A. S.; Shan, Z.; Stach, E. A.; Cyrankowski, E.; Wyrobek, T. J.; Warren, O. *Nat. Mater.* **2006**, *5*, 697−702.
(43) Carpena-Núñez, J.; Yang, D.; Kim, J. W.; Park, C.; Fonseca, L. F. *Nanotechnology* **2013**, *24*, 035701.
(44) Lu, Y.; Peng, C.; Ganesan, Y.; Huang, J. Y.; Lou, J. *Nanotechnology* **2011**, *22*, 355702.
(45) Lu, Y. H.; Liang, S.; Chu, W. Y.; Qiao, L. J. *Intermetallics* **2002**, *10*, 823−827.
(46) Salje, E. K.H.; Palosz, B.; Wruck, B. *J. Phys. C: Solid State Phys.* **1987**, *20*, 4077−4096.
(47) Novak, J.; Salje, E. K. H. *J. Phys.: Condens. Matter* **1998**, *10*, L359−L366.
(48) Zhang, G. F.; Sauvage, X.; Wang, J. T.; Gao, N.; Langdon, T. G. *J. Mater. Sci.* **2013**, *48*, 4613−4619.
(49) Gastien, R.; Sade, M.; Lovey, F. C. *Shape Memory Alloys: Manufacture, Properties and Applications*; Nova Science Publishers: Hauppauge, NY, 2010; pp:145−180.
(50) Gastien, R.; Sade, M.; Lovey, F. C. *Mater. Sci. Eng., A* **2008**, *481*, 518−521.
(51) Condo, A. M.; Lovey, F. C.; Torra, V. *Philos. Mag.* **2003**, *83*, 1479−1493.
(52) Stoiber, J.; Gotthard, R. *Mater. Sci. Eng., A* **1993**, *164*, 443−448.
(53) Wang, R.; Luo, C.; Gui, J.; Ren, Q.; Chen, J. *J. Phys.: Condens. Matter* **1992**, *4*, 2397−2403.
(54) Salje, E. K. H.; Ding, X. D.; Zhao, Z. Y. *Appl. Phys. Lett.* **2013**, *102*, 152909.
(55) Salje, E. K. H.; Zhang, H.; Idrissi, H.; Schryvers, D.; Carpenter, M. A.; Moya, X.; Planes, A. *Phys. Rev. B: Condens. Matter Mater. Phys.* **2009**, *80*, 134114.

DOI: 10.1021/acs.nanolett.5b03483
Nano Lett. XXXX, XXX, XXX−XXX